Article

Compressive Stress Inhibits Proliferation in Tumor Spheroids through a Volume Limitation

Morgan Delarue,[1,*] Fabien Montel,[2] Danijela Vignjevic,[3] Jacques Prost,[1] Jean-François Joanny,[1] and Giovanni Cappello[1]

[1]Physicochimie Curie (Institut Curie/Centre National de la Recherche Scientifique-UMR168/Université Pierre et Marie Curie), Institut Curie, Centre de Recherche, Paris, France; [2]Matière et Système Complexes (Université Paris-Diderot/Centre National de la Recherche Scientifique-UMR 7057), Paris, France; and [3]Institut Curie/Centre National de la Recherche Scientifique-UMR144 /Université Pierre et Marie Curie, Institut Curie, Centre de Recherche, Paris, France

ABSTRACT In most instances, the growth of solid tumors occurs in constrained environments and requires a competition for space. A mechanical crosstalk can arise from this competition. In this article, we dissect the biomechanical sequence caused by a controlled compressive stress on multicellular spheroids (MCSs) used as a tumor model system. On timescales of minutes, we show that a compressive stress causes a reduction of the MCS volume, linked to a reduction of the cell volume in the core of the MCS. On timescales of hours, we observe a reversible induction of the proliferation inhibitor, $p27^{Kip1}$, from the center to the periphery of the spheroid. On timescales of days, we observe that cells are blocked in the cell cycle at the late G1 checkpoint, the restriction point. We show that the effect of pressure on the proliferation can be antagonized by silencing $p27^{Kip1}$. Finally, we quantify a clear correlation between the pressure-induced volume change and the growth rate of the spheroid. The compression-induced proliferation arrest that we studied is conserved for five cell lines, and is completely reversible. It demonstrates a generic crosstalk between mechanical stresses and the key players of cell cycle regulation. Our results suggest a role of volume change in the sensitivity to pressure, and that $p27^{Kip1}$ is strongly influenced by this change.

INTRODUCTION

The importance of the interactions between a tumor and its microenvironment, the stroma, has been recognized for more than a century (1). In most instances, the growth of solid tumors occurring in constrained environments entails a competition for space. The pathways of communication between a tumor and its microenvironment are diverse, but they can broadly be separated into biochemical and mechanical signals. Although the former have been extensively studied (see, for instance, Mueller and Fusenig (2) and Roussos et al. (3)), much less is known about the latter.

The competition for space results in a bidirectional mechanical coupling between the tumor and the stroma: on the one hand, the expanding neoplastic tissue compresses the stroma and thus builds up and stores an internal stress; on the other hand, an active stroma containing contractile myofibroblasts can exert a mechanical stress on the growing tumor (4).

However, given the complexity of these systems, decoupling the effect of biochemical and mechanical interactions is a daunting challenge. A good candidate for such studies is the multicellular spheroid (MCS), introduced by Sutherland et al. (5) as a tumor model system: three-dimensional cellular aggregates that remarkably mimic the relevant in vivo physiological gradients of mitogens, oxygen, or glucose. They have been extensively used (see Hirschhaeuser et al. (6) for a review) as model systems for the study of drug delivery (7), three-dimensional cell proliferation (8), invasion (9), or even angiogenesis (10). Although their mechanical properties might differ from those of tumors, for many purposes, MCSs can be viewed as a tumor subunit. Because they do not have any biochemical crosstalk with their environment, MCSs are ideal to evaluate the impact of mechanical stress on tumor growth (11,12). It has been shown, for example, that the growth of a multicellular spheroid in a confined rigid environment inhibits its own growth (13).

In a previous work, we have studied the influence of a compressive stress applied on MCSs (14–16). We have shown that a compressive stress applied on MCSs grown from the mouse colon carcinoma cell line CT26 drastically and reversibly reduce their growth rate (14,15), and that this reduction is linked to a decrease of cell division in the center of the MCS rather than to an increase of cell apoptosis.

In this article, we dissect the biomechanical sequence caused by a controlled compressive stress. We first show on five different cell lines the generality of the effect observed at the MCS level. On timescales of minutes, we show that a compressive stress causes a reduction of the MCS volume, linked to a reduction of the cell volume in the core of the MCS. On timescales of hours, we observe a reversible induction of the proliferation inhibitor, $p27^{Kip1}$, from the center to the periphery of the spheroid.

Submitted April 2, 2014, and accepted for publication August 18, 2014.

*Correspondence: morgan.delarue@berkeley.edu

Editor: Ewa Paluch.

0006-3495/14/10/1821/8 $2.00

http://dx.doi.org/10.1016/j.bpj.2014.08.031

On the timescales of days, we observe that the cell cycle is blocked at the restriction point. We show that the effect of pressure on the proliferation can be antagonized by silencing $p27^{Kip1}$. Finally, we quantify a clear correlation between the pressure-induced volume change and the growth rate of the spheroid. The temporal sequence of events that we study is completely reversible. It demonstrates a generic crosstalk between mechanical stresses and the key players of cell-cycle regulation. It suggests a role of volume change in the sensitivity to pressure.

MATERIALS AND METHODS

Cell culture, MCSs formation, and mechanical stress

HT29 cells (human colon carcinoma cells, ATCC HTB-38; American Type Culture Collection, Manassas, VA), CT26 (mouse colon adenocarcinoma cells, ATCC CRL-2638; American Type Culture Collection), BC52 (human breast cancer cells, given by D. Lallemand, Institut Curie, Paris, France) and AB6 (mouse sarcoma cells, given by Yeh-Shiu Chu, Institute of Molecular and Cellular Biology, Singapore) are cultured under 37°C, 10% CO_2 in DMEM supplemented with 10% calf serum and 1% antibiotic/antimycotic (culture medium). FHI (murine Schwann cells, obtained from immortalization of primary murine Schwann cells, given by D. Lallemand, Institut Curie) are cultured under the same conditions but with F12:DMEM (1:1) medium, supplemented with 10% calf serum and 1% antibiotic/antimycotic. MCSs are formed in 48-well plates using a classical agarose cushion protocol. When the MCS is formed, Dextran (molecular mass = 100 kDa; Sigma-Aldrich, St. Louis, MO) is added to the culture medium to exert mechanical stress, as previously described in Montel et al. (14,15), at a concentration of 55 g/L to exert 5 kPa, and 80 g/L to exert 10 kPa.

Flow cytometry experiments

Fifteen MCSs are gathered together in 0.9 mL of Trypsin and placed in the incubator for 10 min. Cells are mechanically separated by agitation during 5 min. Trypan Blue measurements have been done to ensure the viability of the cells after dissociation, which is >95%. Trypsin activity is inhibited by addition of 100 μL of calf serum. Ice-cold ethanol (70%) is added dropwise to fix the cells, kept at 4°C for at least 12 h. Extracts are centrifuged at 600*g* for 5 min, then rinsed with ice-cold PBS, centrifuged at 300*g* for 5 min. Cells are resuspended in 300 μL of a propidium iodide (Sigma-Aldrich) solution in PBS at a concentration of 50 μg/mL, and 10 μL of RNase A (1 mg/mL; Sigma-Aldrich) is added. DNA histograms are recorded on a FACSort (BD Bioscience, San Jose, CA) and histogram analyses are performed with MODFIT (Verity Software House, Topsham, ME).

siRNA experiments and Western blots

Approximately 200,000 cells were seeded on 6-well plates the day before the experiment. The cells were transfected using Lipofectamine reagent (Invitrogen, Carlsbad, CA), with or without siRNA. We used four different conditions: no siRNA, a scrambled siRNA, and two different siRNAs targeted against $p27^{Kip1}$ (Dharmacon, Lafayette, CO). The cells were in the transfection medium for 6 h, then resuspended and spheroids were formed out of them.

To perform Western blots, 50 MCSs are placed in 70 μL of RadioImmunoPrecipitation Assay buffer. They are agitated at room temperature for 20 min, then heated at 100°C for 5 min. Laemmli buffer is then added and the solution is heated at 100°C for 5 min. Polyacrylamide gels (NuPAGE 4–12% Bis-Tris gels; Life Technologies, Carlsbad, CA) are run and transferred onto a nitrocellulose membrane. The membrane is rinsed three times in PBST (PBS + 0.05% TWEEN), blocked 1 h with 10% milk and rinsed three times in PBST. Primary antibodies are incubated overnight at 4°C at a typical concentration of 1/2000. Membranes are further rinsed three times in PBST, blocked 30 min, and HRP-secondary antibodies (1/5000) are incubated for 1 h at room temperature. Membranes are rinsed three times and then revealed. To quantify Western blots, we subtract the background and calculate the sum of the intensity for every band of interest. We normalize it by the level of the α-tubulin band. We estimate the minimum and maximum intensity per band, and found that they differ on an average of 10% of the mean value. We take 0.1 × value for the error bar measurement.

Cryosections, immunofluorescence staining, and density profiles

Cryosections, immunofluorescence, and density profiles are performed using the protocol described in Montel et al. (15). Fluorescent images are recorded on an Eclipse microscope (Nikon, Melville, NY), with a Luca S camera (ANDOR Technology, Belfast, UK). Image analysis are performed with a home-made software employing MATLAB (The MathWorks, Natick, MA). Briefly, we localize the position of each nucleus positive for the staining by thresholding the second derivative of the image. Density profiles are obtained by normalizing the radial distribution of the nuclei positive for the staining against the protein of interest by the radial distribution of every nuclei, obtained using a DAPI staining. To have access to the number of nuclei positive for the staining, we sum this density profile over the radius. By tuning the threshold applied on the second derivative, we are able to plot density profiles with no false positive nucleus detected, and with the maximum of nuclei detected, which gives us a minimal and a maximal value for the integral. On average, the error made on the measurement is then taken to be 0.2 × value.

Cell to cell distance

DAPI stainings are obtained as described in the previous section, and images are recorded on a confocal microscope to ensure the same thickness imaged for each sample. To obtain an estimation of the local cell-to-cell distance inside a MCS, we choose an autocorrelation approach, explained in detail in the Supporting Material. Briefly, a small circular region of interest (ROI) is taken randomly inside the DAPI image, at a distance r from the center of the MCS. The autocorrelation of this ROI is done using a Fourier transform approach. We then plot the radial normalized autocorrelation function. Each maximum corresponds to the correlation of a nucleus with one of its neighbors: the first one with itself, the second one with its first neighbor, the third one with its second neighbor, etc. We take an estimation of the cell-to-cell distance $d(r)$ by the average distance with the first neighbor, at the distance r from the center of the spheroid. Eventually, each $(r,d(r))$ point are gathered in a histogram, obtained with bins of the size of the ROI. Each cell-to-cell distance is the median of all the $d(r)$ in the bins, and the error bars correspond to the error on the median of the distribution. Finally, the mean distance corresponds to the mean value of the cell-to-cell distance inside the MCS, and the error bar to the average of the error made for each measurement.

RESULTS

Mechanical stress reduces growth rate of multicellular spheroids on various cell lines

We first check the robustness of the growth-rate reduction of MCSs due to a compressive stress found in Montel et al. (14). We form MCSs from different cell lines: mouse colon

carcinoma CT26, human breast cancer BC52, and human colon carcinoma HT29. Fig. 1 *A* shows the growth of a CT26 MCS, growing from Day 0 to Day 10, with an initial diameter of 200 μm. To test the effect of the cancer stage and type, we also check the growth-rate reduction under a compressive stress for MCS made of Schwann cells (FHI) and sarcoma cells (AB6). We choose these cell lines as a panel of different cancer stages and types. CT26 and HT29 are both colon cancer cells, CT26 showing a more invasive phenotype in vitro. CT26, HT29, BC52, and FHI are all epithelial cancer cells, originating from three different cancer types, whereas AB6 represents sarcoma cancer cells, found in the bulk of tissues.

A biocompatible polymer, Dextran, is added to the culture medium to exert a mechanical stress (Fig. 1 *B*). The biopolymer does not penetrate single cells, and does not affect single-cell growth (14–16). The effect we observe is not an osmotic effect, as is often described in the literature for high osmolarity shocks. When studies mention the osmotic effect, they refer to a high osmolarity osmotic effect, often of salts, which is applied at the single cell level. Moreover, we showed in a previous study that we obtained the same growth result when we interposed a dialysis membrane between the Dextran and the MCS. In this case, the MCS is mechanically compressed by the dialysis membrane, and not directly by the Dextran. The stress that we apply is then a moderate osmotic stress on the outermost layer of cells, which is transmitted as a mechanical stress to the rest of the cells inside the MCS that do not feel the direct interaction with Dextran. Although it has an osmotic origin, this stress acts as a mechanical stress. The compressive stress can be seen as a network stress that tends to reduce the volume occupied by the MCS (14–16). In this regime, Dextran is not affecting single-cell component concentration inasmuch as the reduction of volume observed is small (14). We apply a compressive stress ranging 5–10 kPa. This stress is the order of magnitude of the MCS Young modulus, which can be measured by classical parallel-plate experiments (Marmottant et al. (17) and Manning et al. (18)).

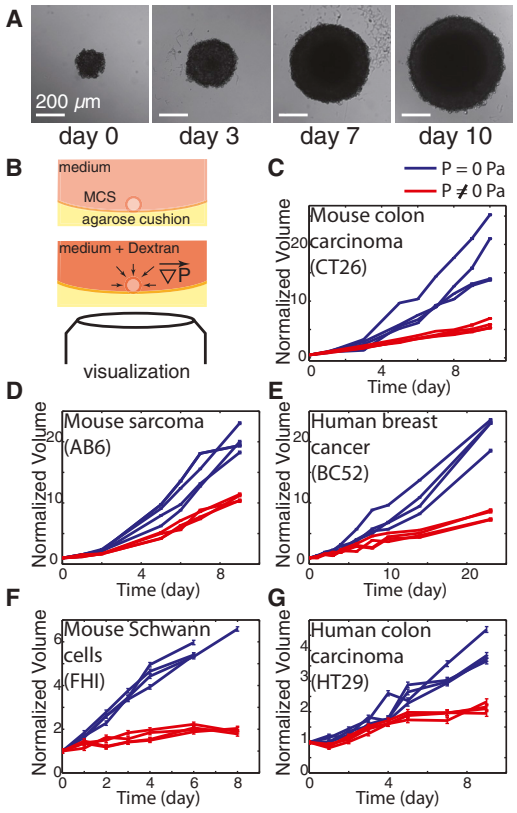

FIGURE 1 Multicellular spheroids and mechanical stress. (*A*) Growth of a CT26 MCS from Day 0 to Day 10 (scale bar, 200 μm). (*B*) Principle of the experiment. Dextran is added to the culture medium, and does not penetrate the MCS. This results in a moderate osmotic stress exerted only on the outermost layer of cells, which is mechanically transmitted to the inner cells, resulting in a compressive stress. (*C–G*) The volume normalized to the initial volume plot as a function of time. The initial volume is ~4 × 10^6 μm^3 for every MCS, and four MCSs are displayed per condition to show reproducibility. (*C–F*) 0 Pa (*blue*) and 5 kPa (*red*); (*G*) 0 Pa (*blue*) and 10 kPa (*red*). The error bars are fixed errors due to measurements, and we estimated that we measured a spheroid diameter with a precision of 10 μm.

Fig. 1, *C–G*, displays the volume of MCSs during growth with or without applied mechanical stress, normalized to the initial volume (~4 × 10^6 μm^3). Despite a quantitative variability between different cell lines, we observe that all spheroids respond to an applied compressive stress with a drastic reduction of their growth rate. Note that the BC52 cell line responds more slowly than the other cell lines, and we need to wait 20 days to see a strong effect of the compressive stress on the growth curve. The same applies to the HT29 cell line. Inasmuch as the spheroids are less stable on longer times, we choose to apply 10 kPa instead of 5 kPa to see a strong effect on the growth curves. The volume is calculated assuming the spheroid's sphericity (14,15), and normalized to the volume before compression.

We proposed in our previous studies a surface growth model derived from Von Bertalanffy (19), where the growth rate is lower in the bulk than at the periphery,

$$\frac{dV}{dt} = kV + (\delta k\lambda)(36\pi)^{1/3}V^{2/3}, \qquad (1)$$

where λ is the thickness of the external proliferative rim, V is the volume of the MCS, $(36\pi)^{1/3}$ $V^{2/3}$ is the MCS surface, $k \leq 0$ is the bulk growth rate, and $\delta k \geq 0$ is the growth-rate increment at the periphery. Each growth curve is fitted with the surface growth model. The extracted parameters k and $(\delta k\lambda)$ are listed in Table S1 in the Supporting Material. The value $(\delta k\lambda)$ has only a weak dependence on stress whereas the bulk rate k decreases by at least a factor 2. These results validate the robustness of our surface-growth model. The growth curves are normalized before compression, and this takes into account all the effects discussed afterwards. This model also suggests that the response of the

cells to stress depends on their positions inside the MCS: it is smaller at the periphery than at the center. In the following, we will focus on HT29, CT26, and BC52 cell lines, and particularly on HT29 for the cell-cycle regulation.

Decrease in cell volume

We investigate the effect of a compressive stress on the variation of the cell volume inside a MCS, on timescales smaller than the cell division time. To evaluate the cell volume, we slice a MCS at different time points after exposure to a compressive stress. Each slice is further stained with DAPI to label the nuclei. The relative distance between the nuclei of adjacent cells ($d(r)$) is measured as a function of their distance r from the center of the MCS, using a two-dimensional position-to-position autocorrelation algorithm. The cell-to-cell distance $d(r)$ is a good proxy for the cell diameter, and hence for the local cell volume. See Fig. S1 in the Supporting Material for more explanation on the method.

Fig. 2 displays the distance $d(r)$ of HT29 cells inside MCSs, at various time points after application of 10 kPa compressive stress. In the absence of mechanical stress, the cell-to-cell distance is roughly constant when controlling for one MCS cell type. Under compression, we observe a heterogeneous reduction of the cell-to-cell distance inside the MCS. At 5 min, the cell-to-cell distance is decreased by roughly 20% in the center of the MCS. A two-tailed t-test yields a p value $p < 0.002$ for the points in the center between $t = 0$ and $t = 5$ min, showing the significance of this decrease. This result is also observed on CT26 and BC52 MCSs under 5 kPa (see Fig. S2). This diameter profile remains unchanged for more than one day after this initial reduction (see Fig. S3). The autocorrelation-based measurement of $d(r)$ is a clear improvement compared to the method used in our previous work (14,15) where we did not see any significant change in cell density. The autocorrelation provides an unbiased estimation of $d(r)$, inasmuch as we do not supervise the identification and localization of each single nucleus. Moreover, the autocorrelation approach gives a better resolution. This enables us to precisely measure the local reduction of cell volume in the center of compressed MCSs.

This rapid cell volume reduction is observed at the level of the MCS where the whole MCS shrinks under compressive stress. This shrinkage is fully compatible with the observed cell volume reduction, and depends on the intensity of the applied stress (see Fig. S4). Note that this cell volume reduction is very large in the MCS compared to the case of individual cells. The compression, contrary to the individual cell scenario, must affect the molecular density of the inner cells.

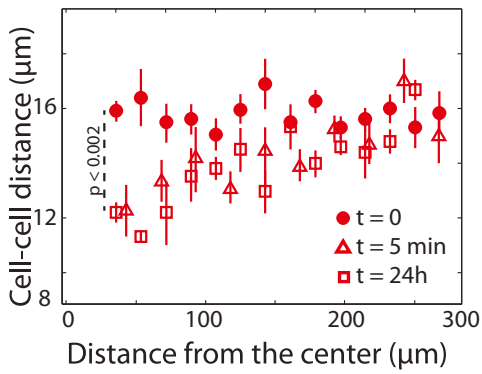

FIGURE 2 Volume reduction through a compressive stress. Cell-to-cell distance plot as a function of the distance from the center for different time points: Day 0 (●), 5 min (△), and Day 1 (□). The error bar obtention is described in the Supporting Material. The experiments have been repeated $N \geq 3$. A two-tailed t-test yields a p value < 0.002 for the points at the center of the MCS, between $t = 0$ and $t = 5$ min. To see this figure in color, go online.

Proliferation inhibition at the restriction point

Huang et al. (20) have shown that individual synchronized endothelial cells submitted to cytoskeletal tension are blocked at the late G1 checkpoint, known as the restriction point. Although the compressive stress has an opposite sign, we address in the following the arrest at the restriction point.

We first perform flow cytometry experiments in which the DNA quantity is assessed. We are able from these data to extract the relative percentage of cells in the G0/G1 phase of the cell cycle. We measure the relative change in this percentage as a function of the applied compressive stress, for cells coming from CT26 MCS and HT29 MCS, but also from CT26 cells cultured individually and submitted to the same concentration of Dextran. We observe in Fig. 3 *A* that

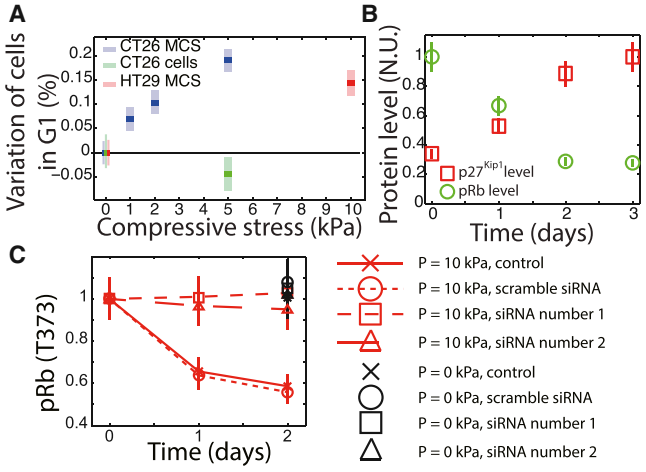

FIGURE 3 Proliferation arrest at the restriction point. (*A*) Results of the flow cytometry experiments. The percentage of cells in G1 is calculated using the software MODFIT, and the variation of this percentage is plot as a function of the applied stress, either for CT26 MCSs (*blue*), CT26 individual cells (*green*), or HT29 MCSs (*red*). (*B*) Level of total pRb and $p27^{Kip1}$ as a function of time. (*C*) Level of pRb (T373) plot as a function of time for different conditions of siRNA and mechanical stress. Each experiment was performed either under 0 kPa or 10 kPa. $N \geq 2$.

the number of cells in the G0/G1 phase of the cell cycle increases as a function of the applied stress in both cell lines when cultured in MCS, but not when cultured individually. This effect then emerges as a three-dimensional property of the spheroids. Note that the other phases of the cell cycle are not affected by a compressive stress (see Table S2). This result shows that cells are blocked in the G1 phase of the cell cycle.

The restriction point is known as the point where the cells commit irreversibly to the cell cycle. It is controlled by the phosphorylation state of the retinoblastoma protein pRb (21). pRb is phosphorylated by cyclin-(cyclin E and cyclin D1)-dependent kinases during G1 to progressively pass the restriction point. This phosphorylation can be inhibited by cyclin-dependent kinase inhibitors such as $p21^{Cip1}$ and $p27^{Kip1}$. These two intrinsically disordered proteins are known to associate with the full repertoire of cyclin-dependent kinases (22). Fig. 3 *B* displays the Western blot analyses for $p27^{Kip1}$ and total pRb. We observe a progressive decrease of pRb level with time, correlated with an overexpression of the kinase inhibitor $p27^{Kip1}$. The level of the cyclins D1 and E, as well as the level of $p21^{Cip1}$, is not affected by the compressive stress (see Fig. S5 *A*). Note that we do not observe any increase of cleaved-caspase 3 over three days, suggesting that there is no direct increase of apoptosis due to the compressive stress on this timescale (see Fig. S6).

We observe that the phosphorylation of pRb is inhibited as well. Among its 16 phosphorylation sites, it has been shown that the phosphorylation of pRb at threonine 373 is a sufficient condition to pass the restriction point (23). We observe that the level of the phosphorylated pRb is correlated with pRb phosphorylated at threonine 373, pRb (T373) (see Fig. S5 *B*), making the latter a good proxy for cell proliferation. To verify that $p27^{Kip1}$ is necessary for this inhibition, we use siRNA targeting $p27^{Kip1}$. We show that we can silence $p27^{Kip1}$ up to two days after the formation of the MCS and the application of the mechanical stress (see Fig. S7). Fig. 3 *C* shows that without siRNA, the level of the pRb (T373) decreases in the control siRNA as well as in the scrambled siRNA. Conversely, when $p27^{Kip1}$ is silenced, we do not observe any decrease of pRb (T373) for two different siRNAs, and its level stays at that without any applied stress. Importantly, we still observe the cell volume decrease in the presence of siRNA.

Taken together, these results demonstrate that a compressive stress inhibits cell proliferation at the level of the restriction point, by an overexpression of the kinase inhibitor $p27^{Kip1}$. In the following, we investigate the spatial changes of $p27^{Kip1}$ and pRb (T373) inside the MCS.

Inhibitory front from the center to the periphery

We investigate the spatial and temporal phosphorylation of pRb at the threonine 373, i.e., proliferation (pRb (T373)) and the overexpression of the proliferation inhibitor $p27^{Kip1}$. Both pRb (T373) and $p27^{Kip1}$ were stained in HT29 and BC52 MCSs, at different time points. Fig. 4 displays images of immunofluorescent staining, first normalized to their highest value, and then averaged over the angle, for pRb (T373) and $p27^{Kip1}$. Below the images, we plot the density profiles for these proteins, calculated as in Montel et al. (14,15). Briefly, we first calculate the radial distribution of this protein for a slice. To do so, we detect every nucleus by thresholding the second derivative of the image with respect to spatial coordinates. We then calculate the radial distribution for every nucleus using the same method. We normalize the protein radial distribution by the nucleus radial distribution, to get a radial density expression of the protein, independent of the slice thickness. Images of the immunofluorescent staining are available in Fig. S8.

We observe that at Day 0 pRb (T373) is more present in the cells at the periphery than in the cells at the center (Fig. 4 *A*), consistent with enhanced cells proliferation at the periphery. Cell proliferation is progressively reduced inside the MCS, in a heterogeneous way: cell proliferation decreases first in the core, and at Day 3, pRb (T373) is only found at the periphery (Fig. 4, *A–D*). We observe that at Day 3, the proliferation profile represented by pRb (T373) remains unchanged for the uncompressed scenario

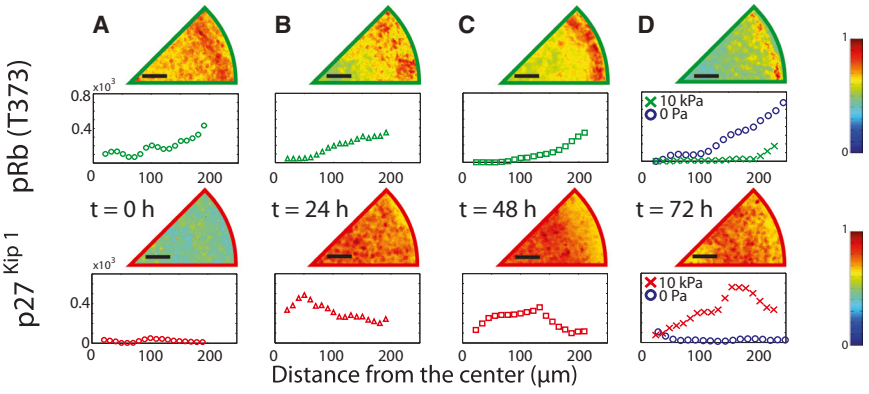

FIGURE 4 Evolution of pRb (T373) and $p27^{Kip1}$. (*Top*) Averaged images of cryosections of HT29 MCSs for the staining of pRb (T373) and $p27^{Kip1}$. The color code indicated is a hot map, blue being the lowest value. The intensity of each image is normalized to its highest value, then averaged over the angle. (*Bottom*) Density profiles of these images. (*A*) $t = 0$ h (○) for $P = 10$ kPa; (*B*) 24 h for $P = 10$ kPa (△); (*C*) $t = 48$ h for $P = 10$ kPa (□); (*D*) $t = 72$ h for $P = 10$ kPa (×) or 0 Pa (○). The densities are given in number of nuclei positive for the staining/μm^2. Each time point was repeated $N \geq 3$. We show the control in the uncompressed scenario only for Day 0 and Day 3, inasmuch as the level does not change.

compared to Day 0. This is consistent with a proliferation reduction due to the applied compressive stress.

The number of cells expressing $p27^{Kip1}$ rapidly increases within the first day, and we observed that $p27^{Kip1}$ is mostly expressed in the center of the MCS at Day 1 (Fig. 4 *B*). The peak of $p27^{Kip1}$ overexpression progressively moves to the periphery of the MCS (Fig. 4, *C* and *D*). This centrifugal inhibitory front correlates well with the drop of pRb (T373). Indeed, $p27^{Kip1}$ being upstream of pRb, it is expected that where the level of the phosphorylated form of pRb represented by pRb (T373) drops, it will be observed that the level of $p27^{Kip1}$ is higher. No increase of $p27^{Kip1}$ is observed three days after the beginning of the experiment in the uncompressed scenario (Fig. 4 *D*, *blue circles*).

These findings on the proliferation reduction and the inhibitory front of $p27^{Kip1}$ were confirmed on the BC52 cell line (see Fig. S9). In MCSs under mechanical stress, only the outermost layers of cells proliferate. This inhibition of proliferation develops as an inhibitory front moving from the center toward the periphery.

Correlation and reversibility

We have shown that a sequential series of events happens before the reduction of cell proliferation. The number of cells overexpressing $p27^{Kip1}$ and pRb (T373), which is estimated from the integral of the cell density, is well correlated to the protein level measured by Western blots (see Fig. S10), making this number a good proxy for the latter. Fig. 5 summarizes the temporal evolution of the mean cell diameter (Fig. 5 *C*), of the number of cells overexpressing the proliferation inhibitor $p27^{Kip1}$ (Fig. 5 *D*) and of the number of proliferative cells expressing pRb (T373) (Fig. 5 *E*) when MCSs are submitted to a compressive mechanical stress (Fig. 5 *B*). We show a sequential response of the cell volume, the overexpression of the proliferation inhibitor, and the reduction of proliferation (Fig. 5 *A*).

The cell diameter responds fast ($\leq$1 min) when we apply a compressive stress. This suggests an elastic response, independent of any signaling or gene expression, and with no induced active response, because at Day 5 the diameter remains the same. The link between the volume change and the mechanical stress is causal: no change would arise without a compressive stress.

The overexpression of $p27^{Kip1}$ responds over a timescale of hours. The temporal response of $p27^{Kip1}$ is consistent with an active synthesis of this protein. $p27^{Kip1}$ and the cell volume are spatially correlated (see Fig. S11). At Day 1, $p27^{Kip1}$ is maximum where the volume is minimum after compression. This correlation suggests that $p27^{Kip1}$ level might be controlled by the cell volume change.

Eventually, the reduction of pRb (T373), i.e., proliferation, happens at the timescale of days. Inasmuch as the cell population is asynchronous, the reduction of proliferation has a delay of approximately one cell cycle, approximately one day for HT29. The link between $p27^{Kip1}$ and pRb (T373) is causal, inasmuch as we show that the effect on proliferation can be antagonized by silencing $p27^{Kip1}$.

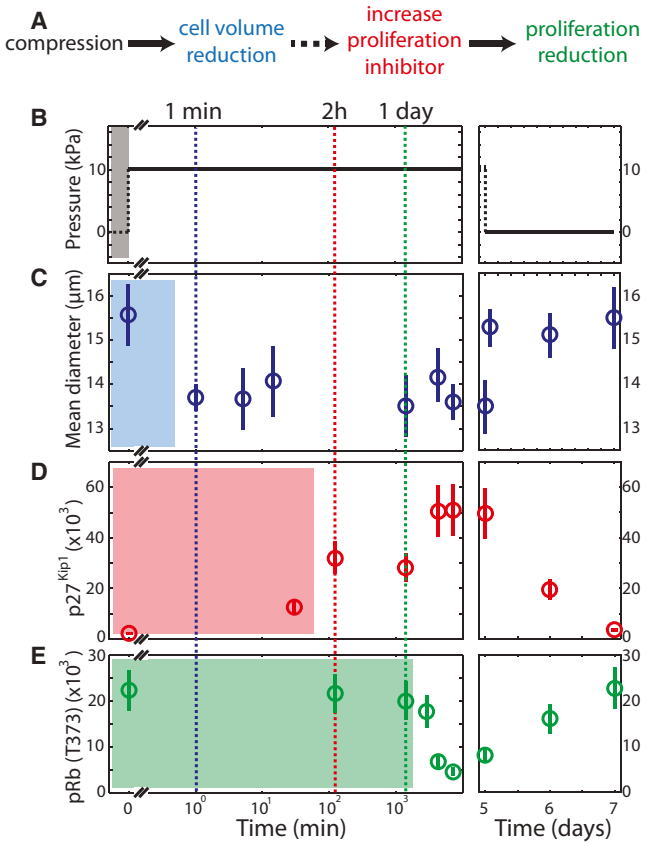

FIGURE 5 Biomechanical sequence and spatial correlation. (*A*) Sequence from compressive stress (*B*) to pRb (T373) reduction (*E*), through mean diameter reduction (*C*) and $p27^{Kip1}$ overexpression (*D*). (*Plain arrow*) Causality between events; (*dashed arrow*) spatial and temporal correlation between events. Note the log scale in time in panels *B*–*E*. Error bar obtention is described in the corresponding paragraphs of the Materials and Methods. To see this figure in color, go online.

This inhibition is reversible. We release the mechanical stress after five days for HT29 MCSs under 10 kPa. We observe that the mean cell diameter resumes in less than a day to the initial value. Note that this relaxation is even faster (~2–3 h) in the case where the spheroid is compressed for 30 min (see Fig. S12). This suggests a passive spongelike mechanism in which cells accommodate their volume to the surrounding stress by water influx/efflux. After relaxation, the number of cells overexpressing $p27^{Kip1}$ progressively decreases as the number of proliferating cells increases to the initial level, showing the reversibility of the inhibition.

Macroscopic correlation between the cell volume and the proliferation rate

We observe that the mechanical stress triggers a volume reduction, followed by and correlated to an increase of

$p27^{Kip1}$, leading to an arrest of proliferation. How can these observations, made at the protein/cell level, be reconciled with the observations made at the MCS level?

We have shown that the growth rate depends on the applied stress (14,15). Fig. 6 displays the initial volume reduction of MCSs, obtained 5 min after the application of the mechanical stress, plotted as a function of the growth rate k obtained from the fitting of the growth curves by the surface growth model. We present here the result for five different intensities of mechanical stress.

We observe a remarkable correlation between the initial volume reduction and the growth rate of the MCS. This observation, which is consistent with all the previous results, suggests that the volume reduction, happening within minutes after the application of the compressive stress, controls the proliferation of the MCS, which is observably measured days after the application of the stress.

DISCUSSION

We have shown that MCSs of various cell lines submitted to a compressive mechanical stress exhibit a reduction of their growth rate. A sequence of events starting from the reduction of cell volume, followed by an inhibitory front of the proliferation inhibitor $p27^{Kip1}$, leads to a reversible reduction of proliferation. Each event is spatially correlated to the previous one, and the reversibility of this sequence indicates that the three events are temporally correlated. Moreover, $p27^{Kip1}$ silencing can antagonize the proliferation reduction, but has no effect on the reduction of the cell volume. This volume change is also spatially correlated to the overexpression of $p27^{Kip1}$. Our results strongly suggest a mechanical control of $p27^{Kip1}$ through a volume change. How can a volume change be translated in an activation of $p27^{Kip1}$? Contrary to the case of individual cells, this stress reduces cell volume, mostly for the inner cells of the MCS. Not all the molecules being soluble, this must entail a change in molecular density.

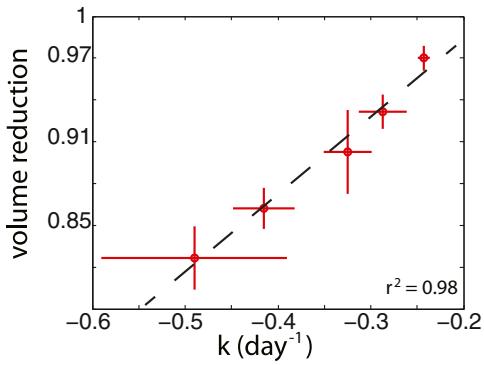

FIGURE 6 Macroscopic correlation between CT26 MCS volume reduction obtained in 5 min and the growth rate obtained by the growth curve fitting over 15 days. A linear regression gives a correlation of 0.98. To see this figure in color, go online.

In 1998, Huang et al. (20) submitted endothelial cells to a mechanical stress. Individual cells were seeded on reduced adherent surfaces to increase their cytoskeletal tension. They observed a proliferation arrest of cells under tension: tension blocks cells in late G1 through an overexpression of $p27^{Kip1}$. The total level of cyclin D1, cyclin E, and $p21^{Cip1}$ was unchanged. In our study, cells are submitted to a compressive mechanical stress. They are, to our knowledge, the first experiments working under compression rather than under tension. Even though the stress has an opposite sign, our results are in agreement with this previous study. In particular, in both cases the mechanical stress affects cell proliferation through an overexpression of $p27^{Kip1}$.

Results on two-dimensional colonies close and after confluency show that at the center of the colony the cell density gets higher, and that the mechanical stress due to its own colony growth leads to a cell volume reduction. This higher density implies a decrease in cell proliferation (24). The results of our work suggest that cell volume change could play a role in the sensitivity to compression. At this point we can only speculate on the link between volume change and p27 activation. The transcription of $p27^{Kip1}$ is controlled by the Forkhead box class O family (FoxO) (25). The phosphorylation of FoxO by the protein kinase B (PKB) is known to inhibit $p27^{Kip1}$ transcription by sequestering FoxO in the cytoplasm (26). It has been shown, however, that the activation of protein kinase C (PKCα isoform in this case) can inhibit PKB inhibition of FoxO (27), which could lead to the transcription of $p27^{Kip1}$.

The PKC family comprises different isoforms that can be separated according to the way they can be activated (28). A subfamily of PKC, like PKCα, requires calcium to be activated. Calcium channels are known to be able to respond to stretching stress (29), and several studies report that cell compression leads to an intercellular increase of calcium concentration (see, for instance, Roberts et al. (30) and Erickson et al. (31)). It has been shown that calcium-dependent PKC activation responds within seconds to a calcium concentration elevation (32). Whether in our case a volume reduction implies an increase of calcium concentration leading to an activation of $p27^{Kip1}$ remains to be proven, however, and would require a distinct study.

More and more studies show that the stroma can play a crucial role in cancer progression. One approach might be to view the microenvironment as a restraining environment for tumor progression. Bissell and Hines (33) report in a review several examples in favor of this approach. We believe that an activated stroma might restrain tumor progression: by exerting an external mechanical stress, the stroma could reduce tumor growth (34).

SUPPORTING MATERIAL

Twelve figures and two tables are available at http://www.biophysj.org/biophysj/supplemental/S0006-3495(14)00936-9.

The authors thank J. Manzi and A. Boin for their help on the Western blotting experiments, and Z. Maciorowski for her help on the flow cytometry experiments. The authors thank E. Hanezzo and S. Monnier for useful discussions. The authors thank the Nikon Imaging Center (Paris, France).

G.C. and F.M. thank the AXA Research Fund, Centre National de la Recherche Scientifique, and l'Institut National du Cancer (INCa) PLBIO for funding.

The research group belongs to the Centre National de la Recherche Scientifique consortium CellTiss.

REFERENCES

1. Paget, S. 1889. The distribution of secondary growths in cancer of the breast. *Lancet.* 1:571–573.
2. Mueller, M. M., and N. E. Fusenig. 2004. Friends or foes—bipolar effects of the tumor stroma in cancer. *Nat. Rev. Cancer.* 4:839–849.
3. Roussos, E. T., J. S. Condeelis, and A. Patsialou. 2011. Chemotaxis in cancer. *Nat. Rev. Cancer.* 11:573–587.
4. Stylianopoulos, T., J. D. Martin, …, R. K. Jain. 2012. Causes, consequences, and remedies for growth-induced solid stress in murine and human tumors. *Proc. Natl. Acad. Sci. USA.* 109:15101–15108.
5. Sutherland, R. M. 1988. Cell and environment interactions in tumor microregions: the multicell spheroid model. *Science.* 240:177–184.
6. Hirschhaeuser, F., H. Menne, …, L. A. Kunz-Schughart. 2010. Multicellular tumor spheroids: an underestimated tool is catching up again. *J. Biotechnol.* 148:3–15.
7. Friedrich, J., C. Seidel, …, L. A. Kunz-Schughart. 2009. Spheroid-based drug screen: considerations and practical approach. *Nat. Protoc.* 4:309–324.
8. Rodríguez-Enríquez, S., J. C. Gallardo-Pérez, …, R. Moreno-Sánchez. 2008. Energy metabolism transition in multi-cellular human tumor spheroids. *J. Cell. Physiol.* 216:189–197.
9. Durek, C., S. Brandau, …, A. Böhle. 1999. Bacillus-Calmette-Guérin (BCG) and 3D tumors: an in vitro model for the study of adhesion and invasion. *J. Urol.* 162:600–605.
10. Bingle, L., C. E. Lewis, …, N. J. Brown. 2006. Macrophages promote angiogenesis in human breast tumor spheroids in vivo. *Br. J. Cancer.* 94:101–107.
11. Venugopalan, G. 2012. Externally applied forces can phenotypically revert malignant breast epithelial structures. *Mol. Biol. Cell.* 23:A1673.
12. Fritsch, A., M. Höckel, …, J. A. Käs. 2010. Are biomechanical changes necessary for tumor progression? *Nat. Phys.* 6:730–732.
13. Helmlinger, G., P. A. Netti, …, R. K. Jain. 1997. Solid stress inhibits the growth of multicellular tumor spheroids. *Nat. Biotechnol.* 15:778–783.
14. Montel, F., M. Delarue, …, J. F. Joanny. 2011. Stress clamp experiments on multicellular tumor spheroids. *Phys. Rev. Lett.* 107:188102.
15. Montel, F., M. Delarue, …, J. Prost. 2012. Isotropic stress reduces proliferation in multicellular spheroids. *New J. Phys.* 14:055008.
16. Delarue, M., F. Montel, …, G. Cappello. 2013. Mechanical control of cell flow in multicellular spheroids. *Phys. Rev. Lett.* 110:138103.
17. Marmottant, P., A. Mgharbel, …, H. Delanoë-Ayari. 2009. The role of fluctuations and stress on the effective viscosity of cell aggregates. *Proc. Natl. Acad. Sci. USA.* 106:17271–17275.
18. Manning, M. L., R. A. Foty, …, E.-M. Schoetz. 2010. Coaction of intercellular adhesion and cortical tension specifies tissue surface tension. *Proc. Natl. Acad. Sci. USA.* 107:12517–12522.
19. Von Bertalanffy, L. 1957. Quantitative laws in metabolism and growth. *Q. Rev. Biol.* 32:217–231.
20. Huang, S., C. S. Chen, and D. E. Ingber. 1998. Control of cyclin D1, $p27^{Kip1}$, and cell cycle progression in human capillary endothelial cells by cell shape and cytoskeletal tension. *Mol. Biol. Cell.* 9:3179–3193.
21. Yao, G., T. J. Lee, …, L. You. 2008. A bistable Rb-E2F switch underlies the restriction point. *Nat. Cell Biol.* 10:476–482.
22. Yoon, M.-K., D. M. Mitrea, …, R. W. Kriwacki. 2012. Cell cycle regulation by the intrinsically disordered proteins p21 and p27. *Biochem. Soc. Trans.* 40:981–988.
23. Lents, N. H., L. L. Gorges, and J. J. Baldassare. 2006. Reverse mutational analysis reveals threonine-373 as a potentially sufficient phosphorylation site for inactivation of the retinoblastoma tumor suppressor protein (pRB). *Cell Cycle.* 5:1699–1707.
24. Puliafito, A., L. Hufnagel, …, B. I. Shraiman. 2012. Collective and single cell behavior in epithelial contact inhibition. *Proc. Natl. Acad. Sci. USA.* 109:739–744.
25. Chu, I. M., L. Hengst, and J. M. Slingerland. 2008. The Cdk inhibitor p27 in human cancer: prognostic potential and relevance to anticancer therapy. *Nat. Rev. Cancer.* 8:253–267.
26. Burgering, B. M. T., and G. J. P. L. Kops. 2002. Cell cycle and death control: long live Forkheads. *Trends Biochem. Sci.* 27:352–360.
27. Chung, Y. W., H. K. Kim, …, P. B. Thock. 2011. Dual function of protein kinase C (PKC) in 12-O-tetradecanoylphorbol-13-acetate (TPA)-induced manganese superoxide dismutase (MnSOD) expression. *J. Biol. Chem.* 286:29681–29690.
28. Newton, A. C. 2010. Protein kinase C: poised to signal. *Am. J. Physiol. Endocrinol. Metab.* 298:E395–E402.
29. Maroto, R., A. Raso, …, O. P. Hamill. 2005. TRPC1 forms the stretch-activated cation channel in vertebrate cells. *Nat. Cell Biol.* 7:179–185.
30. Roberts, S. R., M. M. Knight, …, D. L. Bader. 2001. Mechanical compression influences intracellular Ca^{2+} signaling in chondrocytes seeded in agarose constructs. *J. Appl. Physiol.* 90:1385–1391.
31. Erickson, G. R., L. G. Alexopoulos, and F. Guilak. 2001. Hyperosmotic stress induces volume change and calcium transients in chondrocytes by transmembrane, phospholipid, and G-protein pathways. *J. Biomech.* 34:1527–1535.
32. Oancea, E., and T. Meyer. 1998. Protein kinase C as a molecular machine for decoding calcium and diacylglycerol signals. *Cell.* 95:307–318.
33. Bissell, M. J., and W. C. Hines. 2011. Why don't we get more cancer? A proposed role of the microenvironment in restraining cancer progression. *Nat. Med.* 17:320–329.
34. Basan, M., T. Risler, …, J. Prost. 2009. Homeostatic competition drives tumor growth and metastatic nucleation. *HSFP J.* 4:265–272.